Photovoltaic Cells for Micro-Scale Wireless Sensor Nodes: Measurement and Modeling to Assist System Design

Anand Savanth[1,2], Alex Weddell[1], James Myers[2], David Flynn[1,2], Bashir-Al-Hashimi[1]
[1]Electronics and Computer Science, University of Southampton, UK
[2]ARM Ltd., Cambridge, UK
{asw, bmah}@ecs.soton.ac.uk, {anand.savanth, james.myers, david.flynn}@arm.com,

ABSTRACT

Energy harvesting enables perpetual operation of wireless sensor nodes by scavenging energy from the environment. Light energy harvesting using photovoltaic (PV) cells is preferred as they offer the highest volumetric power output allowing nodes to be as small as possible. However, their power output can be spatially and temporally-variable. This work investigates the performance of cm^2-scale PV cells, and reports on a new measurement and characterization platform. Results show that micro PV cells perform differently from large panels: power is not simply a function of area and light levels, and manufacturing variability can be a major issue. The method presented enables the rational design of micro-scale systems, including their maximum power point tracking circuits, and the evaluation of techniques for energy-neutrality (such as workload throttling) at design-time.

Categories and Subject Descriptors

B.m [**Miscellaneous**]: Design management; B.7.2 [**Integrated Circuits**]: Design Aids—*Simulation*; C.4 [**Performance of Systems**]: Design Studies

Keywords

Energy harvesting, micro-PV cells, SC converters, wireless sensor nodes.

1. INTRODUCTION

To enable mass deployment of wireless sensor nodes (WSN), a number of features are important of which size, cost, power consumption (particularly in sleep mode), and a reliable power supply are critical. For powering energy-neutral WSN, PV energy harvesters generally offer the highest volumetric power output [2], and power conversion and maximum power point tracking (MPPT) techniques for solar energy harvesters are relatively well understood. However, the extent to which available energy varies over time can cause problems for system designers. A system design process generally includes [9] 1) choosing the energy harvesting source, 2) designing matching power conversion circuitry, 3) choosing the type/size of energy storage device, 4) estimating the power budget of the WSN, 5) estimating the size of micro harvester, 6) implementing the most appropriate MPPT technique, and 7) refining for any other system requirements. This complex process affects the cost and ability to deploy a sensor system.

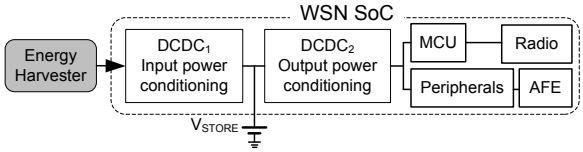

Figure 1: WSN SoC with Energy Harvesting ([9]).

CMOS sub-threshold design techniques allow highly integrated system-on-chip (SoC) WSN to be implemented. Systems that can run with 10's of pico-Joules per cycle have been demonstrated [13], [5] and it is important to ensure such sensor nodes can be powered using micro harvesters of optimal size and power output. In such applications PV cells are used in conjunction with a switching converter ($DCDC_1$ in Fig. 1). Typically, a second DCDC converter is used for converting from V_{STORE} to sub-threshold voltage levels required by the rest of the system.

For perpetual energy-neutral operation of such SoCs it is crucial to have simulation models for PV cells especially for converter designs, evaluating MPPT techniques, and system co-simulations. Prior PV cell modeling efforts ([8], [18] amongst many others) have focussed on large panels with output powers greater than 1mW while, as will be presented later, the characteristics and system dynamics differ considerably when micro PV cells are considered. Previous works exploring PV cell based energy harvesting in the context of self-powered (WSN [4], [10]) use preliminary values from datasheets and iteratively compute remaining model parameters. This work utilizes data from continuous measurement of PV cell current-voltage (IV) characteristics to arrive at a simulation model.

Continuous IV curve logging has been employed in related works such as [7] and [1] but with the primary objective of replaying them to enable repeatable design-time experimental results by emulating energy sources. While [7] use fast 12bit ADCs to capture IV curves within a few milli-seconds, an error of up to 70μA is allowed during emulation, whereas

ENSsys'15, November 1, 2015, Seoul, South Korea..

DOI: http://dx.doi.org/10.1145/2820645.2820653.

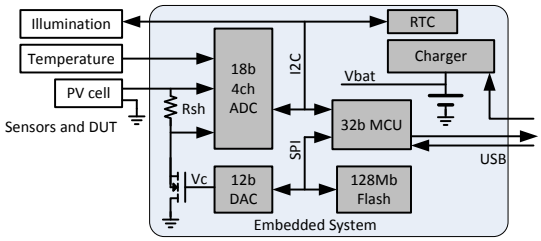

Figure 2: Characterization System.

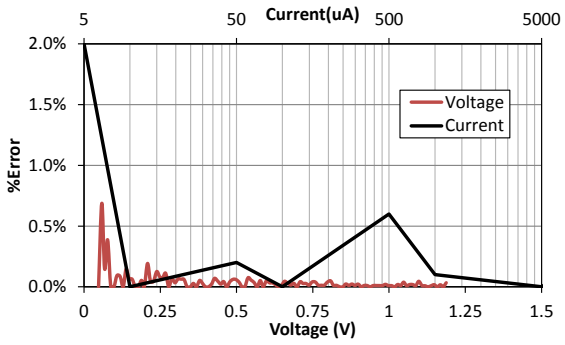

Figure 3: Voltage and current measurement %error.

micro PV cells characterized in this work generate much lower peak currents. Similarly [1] have 10's of mV and 100's of μA emulation error which is limiting in the context of the WSN designs considered here.

This work uses an embedded characterization platform to perform long-term continuous IV measurements on micro PV cells so that post-processing can be used for evaluating a wide range of WSN SoC design choices. The primary objective of this work is to use the data generated to develop SPICE models for micro PV cells. The major contributions of this work are:

- construction of a characterization system for micro PV cells (Section 2), which is applied to a two-diode PV cell model (Section 3),
- performance evaluation of different PV cells over extended periods (Section 4.1),
- evaluation of MPPT techniques applicable to WSN SoC designs (Section 4.2), and consideration of the overall energy budget (Section 4.3).

2. CHARACTERIZATION SYSTEM

A low-cost, portable and precision measurement system is necessary to enable characterising PV cells in large numbers. Sufficient battery and memory storage is required to support data logging over long durations. A convenient method to power such a system would be with batteries that can be recharged over USB since data is eventually transferred to a PC. Thus, desirable features for the characterization system (CS) are high accuracy measurements, large non-volatile memory, easy data transfer interface, rechargeable battery operation and small form-factor.

The block diagram for the CS is shown in Fig. 2. A 1Ah lipo battery which can be charged from 5V sources provides sufficient energy for the CS to record device-under-test (DUT) performance continuously for several days unattended. A 32-bit MCU manages all the data converters and allows PC interface for post processing of data. A light sensor, similar to [16], with integrated IR and broadband spectrum detectors is used for measuring illumination levels and spectral content. A 4-channel 18-bit ADC with internal temperature-compensated voltage reference allows ambient temperature, PV voltage and current measurements at sub-mV and μA accuracy. A 12-bit DAC is used to control the gate voltage (V_c) to a power NFET, which in turn acts as the variable load to the DUT PV cell. All sensors, data-converters and flash memory storage devices use built-in low-power sleep modes. No data is collected under extreme low-light conditions to improve battery and memory usage. Lossless compression and byte-packing is used for better memory utilization. The CS logs time-stamped IV and ambient sensor data and periodically writes the buffered log to the flash device.

Although current measurement is affected by the use of a shunt resistor, temperature, voltage and current values primarily rely on calibration of the 18-bit ADC. Lux measurement uses the standard conversion formula provided in the device datasheet and regression was used to arrive at a correction factor. Post correction, voltage and current agree with calibrated instruments within 0.2% and 2% respectively. The 2% error is for currents below 5μA and for higher values the error is lower (Fig. 3). Since the light sensor covers a wide illumination range, a 20% error in measured values was observed for illumination levels of 200Lux and below while for 1000Lux or greater the error is less than 10%. The CS can complete a 50-point IV sweep within 5 seconds. However, for measurement precision a higher settling time was used. This can cause some of the data points to be inconsistent because of fast temporal changes in illumination. Such data points have been excluded by post-processing (detailed in section 3.1).

3. PV CELL MODELING

Most PV cell modeling methods use information from datasheets to compute the parameter values for simulation models [4]. Methods that rely only on experimental data for obtaining parameters have also been explored; they are often effort-intensive, requiring several IV measurements under controlled conditions [15]. Although IV data for the entire curve is obtained from the CS, an alternative modeling method [6] relies only on measurement of the 'remarkable points', and remaining model parameters are iteratively extracted. Thus, models with better accuracy can be obtained with fewer measurements from a relatively uncontrolled environment. In addition, appreciable accuracy (<0.1% error)

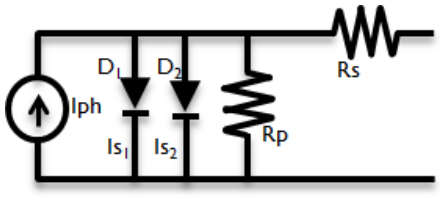

Figure 4: PV cell - two diode model ([3]).

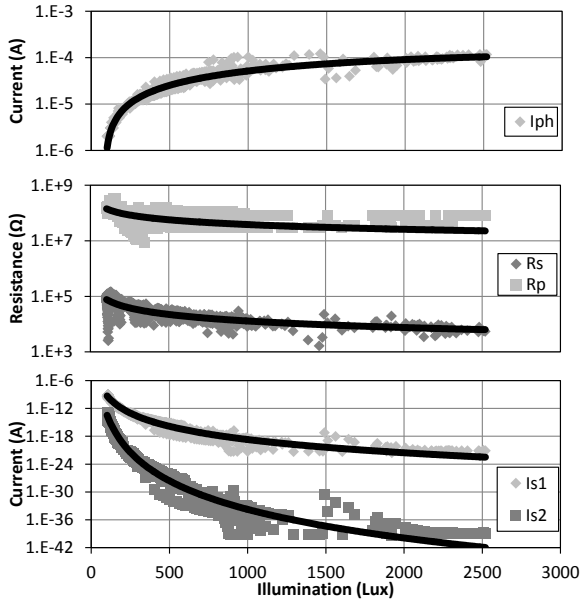

Figure 5: Extracted parameters vs illumination

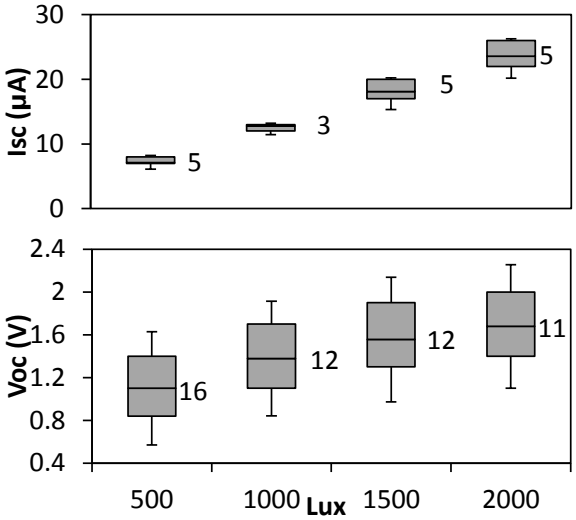

Figure 6: Variation for 9 mono-crystalline PV cells from the same manufacturer. Numeric values indicate ratio of standard deviation over mean as a percentage.

can be attained in the first iteration of the parameter calculation algorithm therefore reducing computation overheads. At these remarkable points, the CS measurement errors are negligible (less than 0.5%).

3.1 PV Cell Parameter Extraction

The two-diode model [3] is considered to be better than the single diode model, particularly for representing the behavior of PV cells under low light conditions. The second diode (D_2 in Fig. 4) which models current due to recombination in the space-charge region (I_{s2}) makes the model more accurate. D_1 models current due to recombination in the quasi-neutral region (I_{s1}). All five model parameters, R_s, R_p, I_{s1}, I_{s2} and I_{ph} can be extracted from measured performance data, which is desirable because the modeled values are tuned for deployment conditions.

Parameter extraction relies on the following set of equations [15] which are computed in this order. With $I_{ph} = I_{sc}$ used as the initial condition, (2) to (5) are computed over multiple iterations (depending on the desired accuracy or computational constraints). However, the logged data must first be pruned to eliminate any inconsistent sweeps. The polarity of K_1, which represents conductance, is an obvious indicator of inconsistent data points.

$$R_{po} = -\Big(\frac{dV}{dI}\Big)_{I=I_{sc}} \tag{1}$$

$$K_1 = \frac{\frac{I_{mpp}}{I_{ph}-I_{mpp}} + log\Big[1 - \frac{I_{mpp}}{I_{ph}}\Big]}{2V_{mpp} - V_{oc}} \tag{2}$$

$$K_2 = log[I_{ph}] - V_{oc}K_1 \tag{3}$$

$$R_s = \frac{V_{mpp} - \frac{I_{mpp}}{[I_{ph}-I_{mpp}]K_1}}{I_{mpp}} \tag{4}$$

$$I_{ph} = I_{sc} + e^{(I_{sc}R_s)K_1 + K_2} \tag{5}$$

Finally R_p, I_{s1}, and I_{s2} are computed using equations (6) to (9). In (7) to (9), q, k and T are the elementary charge, Boltzmann's constant and temperature in Kelvin.

$$R_{so} = -\Big(\frac{dV}{dI}\Big)_{V=V_{oc}} \tag{6}$$

$$I_{s1} = \Big(- I_{sc} + \frac{V_{oc}}{R_{po}} + \frac{2kT}{q(R_{so} - R_s)}\Big)e^{-qV_{oc}/kT} \tag{7}$$

$$I_{s2} = 2\Big(I_{sc} - \frac{V_{oc}}{R_{po}} - \frac{kT}{q(R_{so} - R_s)}\Big)e^{-qV_{oc}/2kT} \tag{8}$$

$$R_p = \left(\frac{1}{R_{po} - R_s} - \frac{qI_{s1}}{kT}e^{q(I_{sc}R_s)/kT} - \frac{qI_{s2}}{2kT}e^{q(I_{sc}R_s)/2kT}\right)^{-1} \tag{9}$$

Figure 5 shows the extracted parameters plotted against illumination, with the continuous lines showing the fitted model. A few points are worthy of mention, to illustrate how the parameters would influence SPICE simulations.

Both resistances decrease with illumination. R_p is 3 orders of magnitude higher than R_s; for the micro-harvester sizes considered here, R_s is of the order of tens of kΩ. The diode currents (I_{s1}, I_{s2}) also decrease with illumination. While this is counter-intuitive, I_{s1} and I_{s2} influence the knee voltage of the diodes causing the PV cell output voltage to be higher at brighter illumination levels.

Another design-critical issue is the variation in PV cells, which must be accounted for in simulation to evaluate best- and worst-case scenarios. Figure 6 shows the spread of open circuit voltage (V_{oc}) and short circuit current (I_{sc}) for nine PV samples measured under varying indoor lighting conditions. The box indicates the spread in the measured samples along with the mean, the whiskers indicate the expected 3-sigma limits. The spread in power at MPP (P_{mpp}) is expected to follow that of V_{oc} because I_{sc} has a relatively tighter distribution (lower sigma-over-mean). The 10-20%

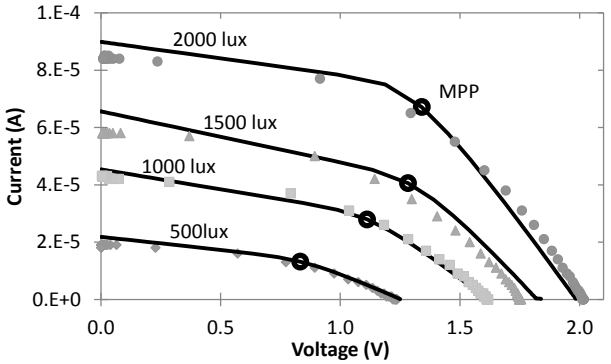

Figure 7: Results obtained from SPICE simulations (continuous lines) with measurements from CS (individual points) and highlighted MPP.

part-to-part variation makes margining WSN designs very difficult. However, it is possible to capture such variation in SPICE using user-defined parameters, which can later be used in Monte-Carlo sweeps for statistical yield analysis and also for evaluating worst-case operating conditions.

3.2 SPICE Simulations

The SPICE model for the PV cell uses fitting functions for each parameter, as a function of illumination and temperature. The fitted functions from Figure 5 feed into the schematic shown in Figure 4. The resulting sub-circuit was simulated using HSPICE®, a standard EDA tool used for SoC designs. Simulated and measured values of the remarkable points are compared in Table 1. The P_{mpp} and V_{oc} readings agree within 10%, while the error for I_{sc} (particularly at low light levels) is 18%.

Further, the PV model was simulated with an ideal current source as load under different illumination settings and IV curves were obtained. These are compared with the measured data in Figure 7. The expected use case of the model is to simulate switched capacitor (SC) converters with the PV cell model sub-circuit as the power source with illumination set as a simulation parameter. Also, transient simulations can be carried out by setting the illumination as a function of piece-wise-linear voltage source to evaluate metrics such as speed of MPPT convergence, power overheads and relative gains in harvested energy for different MPPT techniques.

4. RESULTS AND ANALYSIS

Multiple CS units were fabricated and used to evaluate several high-efficiency surface-mount monocrystalline PV cells from different manufacturers. The cells were measured both indoors and outdoors, over a period of several days. The results are described first, followed by a discussion of the fractional open circuit voltage (FOCV) MPPT technique and finally a consideration of the PV cell area and WSN energy budget.

Table 1: PV cell measured and simulated remarkable points for different illumination settings

lux	V_{oc} (V)			I_{sc} (μA)			P_{mpp} (μW)		
	M	S	%E	M	S	%E	M	S	%E
500	1.25	1.24	1	22	18	18	10	11	9
1000	1.61	1.62	0.4	45	43	5	32	31	3
1500	1.84	1.76	5	66	58	12	48	52	8
2000	1.98	1.98	2	90	84	7	84	90	7

M=measured, S=simulation, E=Error

4.1 Characteristics of Harvested Energy

Figure 8 shows plots of data collected using the CS from a 22 x 7mm monocrystalline PV cell over a four-day period, at the rate of one sweep every two minutes. Indoor office illumination was used although, as in a real-world scenario, additional scattered illumination from over-cast daylight was available during measurements. It is worth noting that temperature is relatively constant ($\pm 5^{\circ}$C) and V_{mpp} changes are attributable solely to illumination. The availability of raw IV data removes ambiguity in the maximum power point location, and allows potential strategies for MPPT to be assessed off-line.

Assuming an ideal MPPT technique, the maximum power that can be extracted from the DUT is shown, along with the voltage levels at which P_{mpp} is obtained (V_{mpp}). This is a key input for SC converter design: it enables the estimation of conversion ratios and cold-start voltages. P_{mpp} integrated with time would be the ideal-case energy budget of the WSN operating for the same duration.

In practice however, only a fraction of this ideal energy can be used. Firstly, conventional circuits fail to use harvested energy at low voltages and about 30% of the aggregate energy is available at $V_{mpp} < 0.3V$. SoC implementations of SC converters demonstrate functional voltage limits as low as 0.14V [11] but for voltages below 0.35V the conversion efficiency is limited to 50%. Thus, there is a further energy loss due to the non-ideal harvester-converter interface. Secondly, power conversion losses in the conditioning circuitry will limit P_{mpp} utilization even when $V_{mpp} > 0.3V$. A comprehensive review of integrated implementations of SC converters [17] shows upto 90% conversion efficiency under best-case conditions. However, the temporal variations of V_{mpp} limit conversion efficiencies; this calls for careful choice of harvester and converter design parameters.

The lower voltage limit on SC converters could potentially be overcome by connecting several (N_s) cells in series, to increase the PV output voltage. To evaluate the trade-offs, PV cells with N_s=1 and 2 were measured under similar illumina-

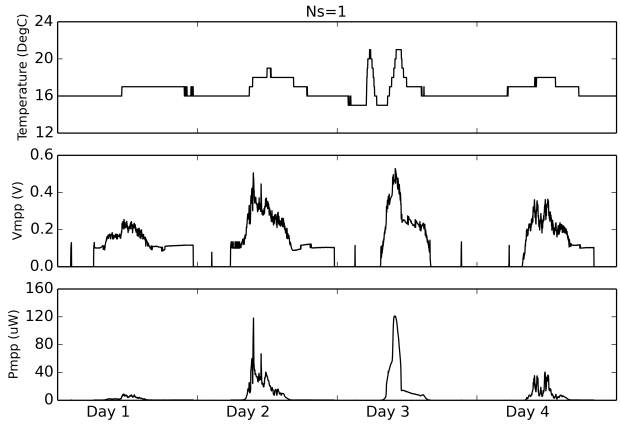

Figure 8: Plot of energy harvested over six days.

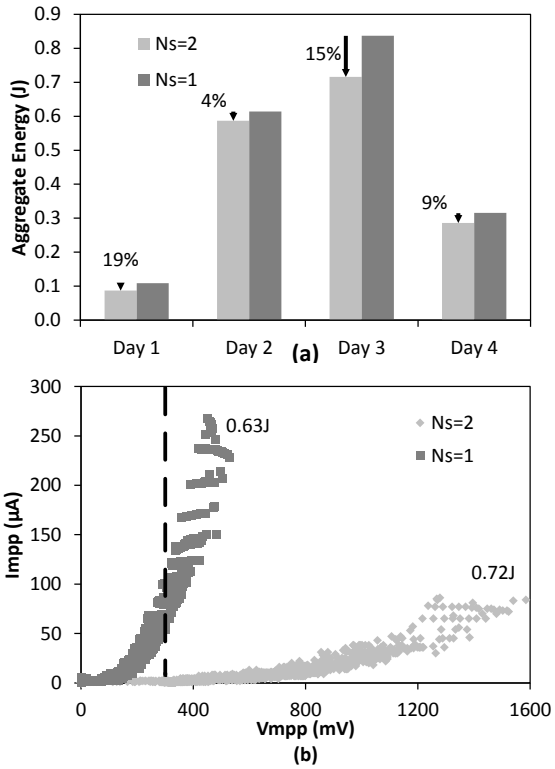

Figure 9: Aggregate energy from PV cell with N_s=1,2 (a) Relative energy harvesting performance and (b) V_{mpp} vs I_{mpp}.

tion and temperature conditions and the results are shown in Fig. 9. The daily-total energy indicates that output from cells with N_s=2 is 5 to 20% lower than cells with N_s=1. Therefore, for higher harvesting efficiency, N_s=1 would be preferred. However, for SC converters with a 300 mV lower voltage limit, the result favours cells with N_s=2. This is highlighted in Fig.9(b) which shows cells with N_s=2 having higher voltage V_{mpp} compared to the cell with N_s=1, but lower current I_{mpp}. If the aggregate is recomputed with the integral lower limit at 300mV (dashed line in Fig.9(b)) then the harvested energy from N_s=2 cells is 6-100% higher than that obtained from cells with N_s=1.

4.2 MPPT Overheads

Several MPPT techniques have been proposed for large panels where the power available justifies expending a small percentage on MPPT circuitry, but in the context of WSN where the overall power budget is of the order of tens of μW, the choice of MPPT technique is crucial. The FOCV technique is preferred [12] because of lower implementation costs (power and area). The drawback with this technique is that the load needs momentary disconnection to measure V_{oc}. This is usually overcome by using decoupling capacitance. The bigger challenge is in deciding the optimal value of the fraction (K_{opt}). Three different micro PV cells were evaluated against ideal P_{mpp} obtained from the family of measured IV curves. Two of the cells used N_s=2 and show contrasting fractions at which the P_{mpp} is close to ideal. Figure 10 shows this result, along with PV1 which has N_s=1.

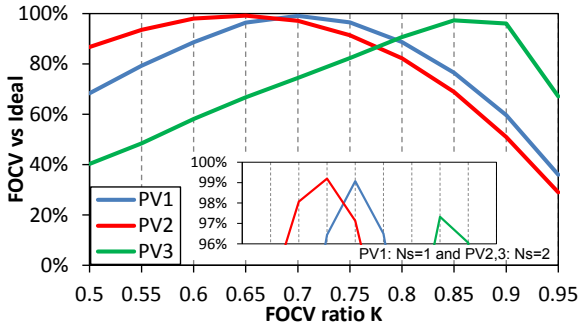

Figure 10: Fractional V_{oc} MPPT technique evaluation.

Cells PV1 and PV2 show K_{opt}=0.65 and 0.7 while PV3 has a fraction close to 0.9. This is attributed to the fill-factor of the PV cells. For the data shown in Figure 10, the power difference between ideal and K_{opt} case is about 1-3% of ideal. The implementation cost for the FOCV method is not accounted. Typically this cost is due to additional power loss in the divider resistors, comparators and other tuning circuitry.

4.3 WSN Energy Budget Estimation

Unlike many computation platforms, WSNs benefit from a relatively fixed repetitive workload for their lifetime. Thus, knowledge of the end application and characteristics of the energy harvester can be used to optimize sensor node sizes design-time. It is however challenging to estimate and optimize for the worst and best case scenarios.

Consider, for example, the energy reported by the example WSN SoC in [14]. While running software code the active energy is 12 pJ/cycle and the frequency is 1MHz. The sleep power is 80nW. Assuming 50% SC converter efficiency and 3000 cycles for one loop of activity the active energy is (12 x 2 x 3000) 72nJ expended over 3ms. Sensor workloads are heavily duty-cycled, and one must account for retention or sleep power. Assuming a 10:1 sleep:active duty-cycle, 80nW retention power translates to (80n x 2 x 30m) 4.8nJ. So the total energy for one loop of activity and sleep (workload) is 76.8nJ spent over 33ms. From Figure 9(a), the lowest energy daily-total obtained with V_{mpp} > 300mV, is 85mJ over 24hrs. One must also factor in MPPT efficiency for obtained energy. The data in Figure 9(a) assumes an ideal MPPT implementation. If the MPPT implementation was 75% efficient, the energy available reduces to 63mJ over 24 hours. So the aforementioned workload can run continuously for 0.8 million loops or 8 hours. This discussion suggests that, within the limits of assumptions made, more than three times the PV cell area would be necessary for perpetual operation of the example WSN SoC. However, energy is also lost due to self-discharge in the energy storage devices, temperature, and other non-ideal phenomena.

Alternatively, considering best-case numbers from Figure 9(a), the cell area works out to about half, for a 24 hour period of energy-neutral operation. This is a 6x difference between the worst and best case scenarios. It is noted that the PV output is not necessarily a linear function of area. This discussion also does not consider part-to-part variation of PV cells which would otherwise add to the design margins.

If the sensor hardware is fixed, then the duty-cycle can be throttled to ensure a 24hr operation. In the example stated earlier, a 30:1 duty-cycle would provide a 24hr operation for the same PV cell area or sensor volume.

Summarily, the proposed method and model helps draw out specifications for SC converters, choose the appropriate MPPT technique and specify design requirements for MPPT implementations. The overall view helps estimate WSN energy budgets and workloads for the sensor. The energy estimate also has implications on the type and size of battery or super-capacitor that can be used in a sensor node design. By relying on field measurements, addressing variation and potential worst-case conditions this modeling method helps design integrated WSNs with tighter tolerances at lower costs.

5. CONCLUSIONS

WSNs must rely on energy harvesting for perpetual operation and longer active lifetimes. The design of energy-neutral WSNs with small form factors would be less optimal without design-time verification of extreme and typical corner cases. This work has presented a measurement and characterization platform for micro PV cells which provides much-needed data for generating a PV model to be used for WSN SoC co-simulations. In addition, the data helped identify key differences in conventional rules-of-thumb that are applied to large PV panels. Also, example analysis showed how MPPT techniques, their implementation and WSN energy budgets can be cost-effectively evaluated using data generated by the characterization platform.

6. ACKNOWLEDGEMENTS

Authors acknowledge Shidhartha Das for support with SPICE modeling and Andrew Kufel for assistance with fabrication.

7. REFERENCES

[1] S. Bobovych, N. Banerjee, R. Robucci, J. P. Parkerson, J. Schmandt, and C. Patel. SunaPlayer: High-accuracy Emulation of Solar Cells, 2015.

[2] S. Boisseau, G. Despesse, and B. A. Seddik. Electrostatic Conversion for Vibration Energy Harvesting, Oct. 2012.

[3] D. Chan and J. Phang. Analytical methods for the extraction of solar-cell single- and double-diode model parameters from I-V characteristics, Feb 1987.

[4] D. Dondi, D. Brunelli, L. Benini, P. Pavan, A. Bertacchini, and L. Larcher. Photovoltaic cell modeling for solar energy powered sensor networks, June 2007.

[5] M. Fojtik, D. Kim, G. Chen, Y.-S. Lin, D. Fick, J. Park, M. Seok, M.-T. Chen, Z. Foo, D. Blaauw, and D. Sylvester. A Millimeter-Scale Energy-Autonomous Sensor System With Stacked Battery and Solar Cells, March 2013.

[6] M. Glass. Improved solar array power point model with SPICE realization, Aug 1996.

[7] J. Hester, T. Scott, and J. Sorber. Ekho: Realistic and Repeatable Experimentation for Tiny Energy-harvesting Sensors, 2014.

[8] Y.-P. Huang. A Rapid Maximum Power Measurement System for High-Concentration Photovoltaic Modules Using the Fractional Open-Circuit Voltage Technique and Controllable Electronic Load, Nov 2014.

[9] J. Jeong and D. Culler. A Practical Theory of Micro-solar Power Sensor Networks, Nov. 2012.

[10] J.-E. Jeong, J.-H. Bae, J. Lee, C. S. Lee, J.-H. Chun, and K.-W. Kwon. A Photovoltaic Power Management System using a Luminance-Controlled Oscillator for USN Applications, 2013.

[11] W. Jung, S. Oh, S. Bang, Y. Lee, D. Sylvester, and D. Blaauw. A 3nW fully integrated energy harvester based on self-oscillating switched-capacitor DC-DC converter, Feb 2014.

[12] K. Kadirvel, Y. Ramadass, U. Lyles, J. Carpenter, V. Ivanov, V. McNeil, A. Chandrakasan, and B. Lum-Shue-Chan. A 330nA energy-harvesting charger with battery management for solar and thermoelectric energy harvesting, Feb 2012.

[13] J. Kwong, Y. Ramadass, N. Verma, M. Koesler, K. Huber, H. Moormann, and A. Chandrakasan. A 65nm Sub-Vt Microcontroller with Integrated SRAM and Switched-Capacitor DC-DC Converter, Feb 2008.

[14] J. Myers, A. Savanth, D. Howard, R. Gaddh, P. Prabhat, and D. Flynn. An 80nW retention 11.7pJ/cycle active subthreshold ARM Cortex-M0+ subsystem in 65nm CMOS for WSN applications, Feb 2015.

[15] M. C. D. Piazza and G. Vitale. Photovoltaic sources - modeling and emulationl, 2013.

[16] J. Sarik, K. Kim, M. Gorlatova, I. Kymissis, and G. Zussman. More than meets the eye - A portable measurement unit for characterizing light energy availability, Dec 2013.

[17] G. Villar-Pique, H. Bergveld, and E. Alarcon. Survey and Benchmark of Fully Integrated Switching Power Converters: Switched-Capacitor Versus Inductive Approach, Sept 2013.

[18] U. Zimmermann and M. Edoff. A Maximum Power Point Tracker for Long-Term Logging of PV Module Performance, Jan 2012.